SANDIA REPORT
SAND2019-XXXX
Unlimited Release
Printed XXXX 2019

Diffusive Properties of UNESE Core Samples via Continuously Monitored Mass Spectroscopy

Matthew J. Paul and Scott T. Broome

Prepared by
Sandia National Laboratories
Albuquerque, New Mexico 87185 and Livermore, California 94550

Sandia National Laboratories is a multimission laboratory managed and operated by National Technology and Engineering Solutions of Sandia, LLC, a wholly owned subsidiary of Honeywell International, Inc., for the U.S. Department of Energy's National Nuclear Security Administration under contract DE-NA0003525.

Issued by Sandia National Laboratories, operated for the United States Department of Energy by National Technology and Engineering Solutions of Sandia, LLC.

Available to DOE and DOE contractors from
U.S. Department of Energy
Office of Scientific and Technical Information
P.O. Box 62
Oak Ridge, TN 37831

Telephone: (865) 576-8401
Facsimile: (865) 576-5728
E-Mail: reports@osti.gov
Online ordering: http://www.osti.gov/scitech

Available to the public from
U.S. Department of Commerce
National Technical Information Service
5301 Shawnee Rd
Alexandria, VA 22312

Telephone: (800) 553-6847
Facsimile: (703) 605-6900
E-Mail: orders@ntis.gov
Online order: https://classic.ntis.gov/help/order-methods/

This page is intentionally left blank.

SAND2019-XXXX
Printed XXXX 2019
Unlimited Release

Diffusive Properties of UNESE Core Samples via Continuously Monitored Mass Spectroscopy

Matthew J. Paul[1] and Scott T. Broome[2],
[1]Geochemistry (08865), [2]Geomechanics (08864)
Sandia National Laboratories
PO Box 5800, MS 1033
Albuquerque, New Mexico 87185-1033

ABSTRACT

The transport properties of porous geological media are of fundamental importance when modeling the migration of chemical and radiological species in subterranean systems. Due to their relatively high mobility, short-lived noble gas species are of particular interest as detection of these species at the surface is a tell-tale indicator of recent nuclear activity. However, determining the diffusivity of these species is challenging due to their inert and transparent nature, requiring chemically insensitive techniques, such as mass spectroscopy, to quantify noble gas concentrations. The work described herein details recent advances in the methodology for determining diffusivity on porous media and results obtained on samples relevant to the UNESE project.

ACKNOWLEDGEMENTS

The authors would like to thank Joshua Feldman, Kris Kuhlman, and Jason Heath for their thoughtful discussions during the experimental design phase and for their critical reviews of the report.

The authors would like to thank the National Nuclear Security Administration, Defense Nuclear Nonproliferation Research and Development, for sponsoring this work. We would also like to thank the Underground Nuclear Explosion Signatures Experiment team, a multi-institutional and interdisciplinary group of scientists and engineers, for its technical contributions.

TABLE OF CONTENTS

FIGURES

TABLES

NOMENCLATURE

Abbreviation	Definition
CTBT	Comprehensive Nuclear Test-Ban Treaty
PW	Partially Welded Tuff
SW	Strongly Welded Tuff
UNE	Underground Nuclear Explosion
UNESE	Underground Nuclear Explosion Signatures Experiment
VN	Vitric Non-Welded Tuff
ZN	Zeolitic Non-Welded Tuff

GLOSSARY OF SYMBOLS

Symbol	Definition
$\bar{A}$	Cross-section Area of Porous Media Sample
b_i	Klinkenberg Correction Factor of Species i
C	Vacuum Conductance
c	Index for Carrier Gas Species
d	Pore Diameter
D_{ij}	Binary/Maxwell-Stefan Diffusivity between Species i and j
D_{iK}	Knudsen Diffusivity of Species i
$\mathfrak{D}_i$	Effective Diffusivity of Species i
ε	Porosity
$\bar{g}$	Gravitational Field Strength
I_i	Ion Current of Species i
i	Index of Tracer Gas Species
κ	Effective Permeability
κ_∞	Intrinsic/Liquid Permeability
K	Pneumatic Conductance
k	Eigenvalue
λ	Mean Free Path
L	Length of Porous Media Sample
ℓ	Index for Lower Chamber
η	Dynamic Viscosity
μ_i	Chemical Potential of Species i
n	Molar Concentration
N	Molar Quantity
$\dot{N}$	Molar Flow Rate
$\overline{N}$	Molar Flux
P	Pressure

Symbol	Definition
$\mathcal{p}$	Index for Porous Media Flow
Q	Obstruction Factor
$\mathcal{q}$	Index for Quadrupole Flow
ρ	Mass Concentration
R	Ideal Gas Constant
σ	Gas Collision Diameter
τ	Tortuosity
T	Temperature
u	Linear Velocity
$\mathcal{u}$	Index for Upper Chamber
y_i	Molar Fraction of Species i
V	Volume of Chamber

1. INTRODUCTION

A critical component of the Underground Nuclear Explosion Signatures Experiment (UNESE) program is a realistic understanding of post-detonation processes and changes in the environment that produce observable physical and radio-chemical signatures. As such, knowledge of the pre- and post-UNE (underground nuclear explosion) rock and fracture properties are essential parameters for any UNESE test bed. In response to the need for accurate modeling scenarios of these observations, an experimental program was developed to determine the diffusive properties of core near site U12p.03 of the Nevada National Security Site.

Gas transport in porous media has been studied for a variety of purposes for more than a century. The application areas have varied, from soil aeration, optimizing catalytic pellets, natural gas extraction, carbon sequestration, or contaminant transport. Despite this, due to the complexity and variety of porous media, no one model of transport has proven adequate. The complexity further increases with the addition of a liquid phase, which is nearly ubiquitous in the crust of the earth.

The work herein focuses on attempts to characterize the diffusive flow of the noble gases argon and xenon, as well as the inert molecular gas, sulfur hexafluoride. The noble gases are chosen, not for their inertness, although they provide insight into the fundamental science, but as they are either fission or activation products produced in an underground nuclear explosion. The production, transport, and detection of radionuclides form one of primary methods of enforcing the pending comprehensive nuclear-test-ban treaty (CTBT) (United Nations 1996). In addition, sulfur hexafluoride, being exceedingly inert for a molecular gas, has been historically used as geological tracer and as a chemical simulant for xenon transport (Carrigan, et al. 1996) (Olsen, et al. 2016).

In the case of the noble gases, the chemical inertness and lack of molecular bonds causes these species to be non-trivial to quantify in trace quantities. Mass spectroscopy is one successful method (Paul, Biegalski, et al. 2018), given its nearly universal applicability to all chemical species. However, relying on the traditional methods of Ney and Armistead requires tedious batch sampling (Ney and Armistead 1947). The work presented here describes advances in the methodology to compensate for the material withdrawn by continuously monitored mass spectroscopy.

Core samples were obtained pre-UNE (vertical core hole UE-12p#4), post-UNE within tunnel lithology (U12p.03 RE-7 drilled June 2017), and post-UNE (vertical core hole UE-12p#7 drilled May 2018). U12p.03 RE-7 was drilled 30 degrees above horizontal from portal U12p.02 to intersection of chimney of UNE in U12p.03. UE-12p#7 was drilled vertically from the land surface on Aqueduct Mesa down to approximately 280 feet from U12p.03 working point. Pre- and post-UNE core holes are shown in Figure 1-1. In agreement with geologists and modelers at collaborating laboratories, pre- and post-UNE core was categorized into four lithologies: (1) partially welded tuff (PW); (2) strongly welded tuff (SW); (3) vitric nonwelded tuff (VN); and (4) zeolitic nonwelded tuff (ZN). All core from U12p.03 RE-7 is ZN; drilling at 30 degrees above horizontal did not reach VN lithology.

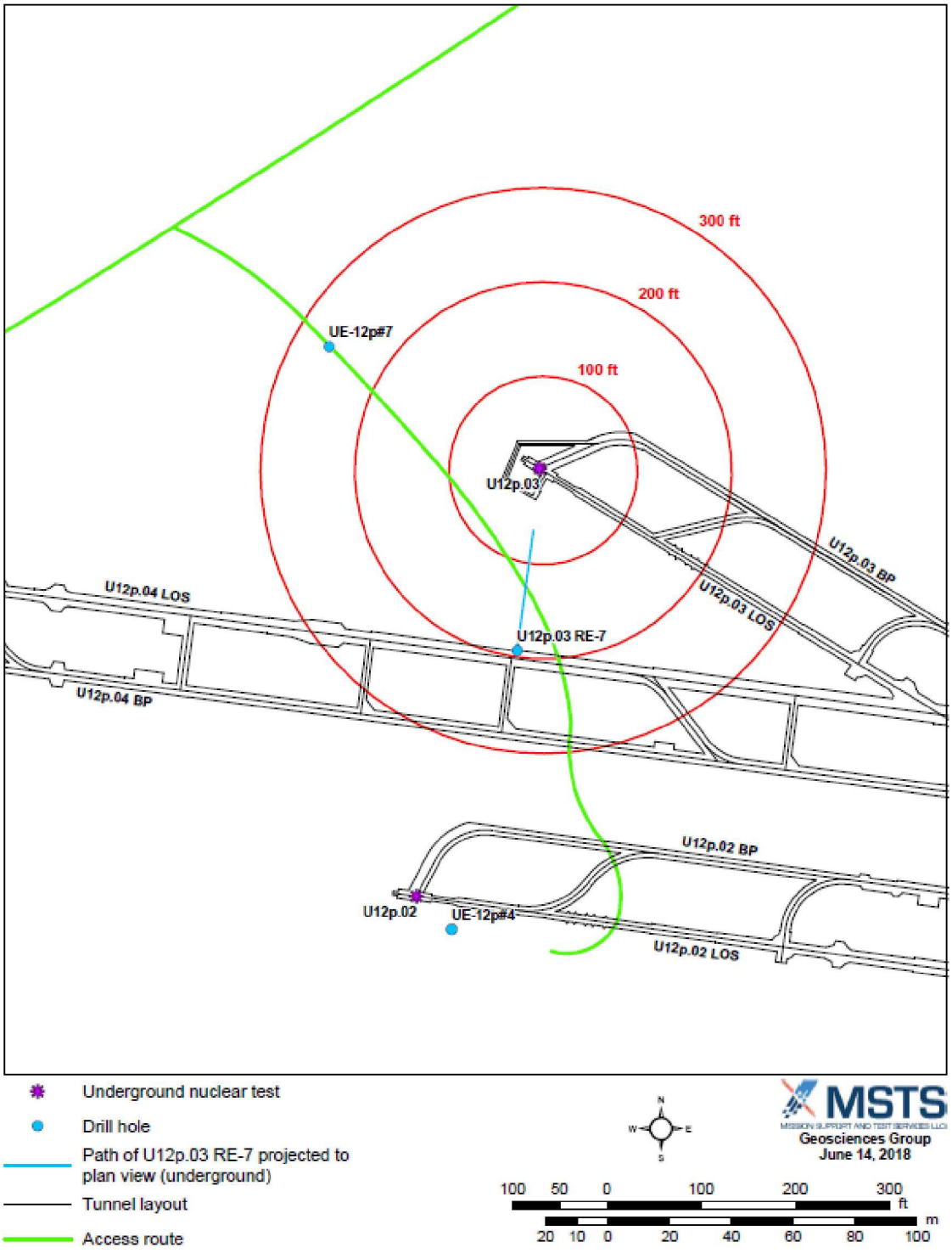

Reference Map for the UNESE Aqueduct Mesa Surface Test Bed

Figure 1-1. Map depicting location of core holes UE-12p#4 (pre-UNE), U12p.03 RE-7 (post-UNE), and UE-12p#7 (post-UNE)

2. THEORY

All transport processes describe the rate at which a non-equilibrium system tends towards thermodynamic equilibrium. From the kinetic theory of gases, the classical thermodynamic properties of density, pressure, and temperature can be related to the number density, momentum, and kinetic energy of an ensemble of gas particles. As mass, momentum, and energy are conserved and as kinetic energy is precisely defined by mass and momentum, knowing two of these parameters is sufficient to determine the third.

Exploring the equilibrium distribution of these parameters is not necessary here. It is sufficient to state that, through statistical approximations, the classical thermodynamic concepts of pressure and temperature are directly related to momentum and kinetic energy. Combined with the relationship to kinetic energy, the ideal gas law is confirmed mathematically:

$$n = \frac{N}{V} = \frac{P}{RT}$$

Here, n, refers to the molar concentration. That is, the molar quantity, N, confined in the volume, V. P is then the total pressure, R, the ideal gas constant, and T, the absolute temperature. The molar concentration of an ideal gas is thereby a function of pressure and temperature only.

However, the ideal gas law is, strictly speaking, only accurate at thermodynamic equilibrium. If the ensemble of particles is not at an equilibrium distribution, through chaotic collisions, the ensemble will spontaneously trend towards equilibrium. Provided with small enough perturbations, the rate at which the distribution approaches equilibrium is independent of the other properties (Chapman and Cowling 1970). This leads to the transport phenomenon of mass diffusivity, momentum diffusivity (viscosity), and thermal diffusivity (conductivity). Each of these transport properties is related to the likelihood of collision with other gas particles and the magnitude of the collision. The mean free path between gas-gas collisions, λ is a function of the hard sphere of diameter σ, and molar concentration (O'Hanlon 2003). Or, using the ideal gas equation of state, this is equivalently a function of temperature and pressure:

$$\lambda = \frac{1}{\sqrt{2}\pi\sigma^2 n} = \frac{RT}{\sqrt{2}\pi\sigma^2 P}$$

Note that the mean free path is not dependent upon the mass of particle. Thus, provided that the particle diameter is similar, the mean free path will be similar for all gas species. While this is a reasonable approximation, real molecules have far more complex interactions, generally following a long-distance attraction with a short-distance repulsion.

In porous media, the situation is somewhat more complex as interactions with the solid phase become significant when the pore dimensions are on the same scale as the random gas particle motion. The non-dimensional Knudsen number, Kn, is defined to compare these length scale; this is simply the ratio of the mean free path, λ, to the pore diameter, d:

$$\mathrm{Kn} = \frac{\lambda}{d}$$

Where the Knudsen number is above unity, collisions with the solid phase exceed the number of collisions with other gas particles. From a transport perspective, collisions with the solid phase differ from gas-gas collisions substantially. The solid phase is composed of a lattice of an immense number of atoms. In contrast, in a gas-gas collision, the particles are of a similar mass. Therefore, the kinetic energy transferred is very high for gas-gas collisions and very low for gas-solid collisions. Similarly, the recoil velocity after a gas-solid collision is very different than for a gas-gas collision. This results in very different transport properties.

To some extent, the situation is less complex at large Knudsen number, as only one type of collision – gas-gas – predominates. In contrast, in the transition region, gas-gas collisions predominate in the center of the pore while gas-solid collisions predominate near the edges. This results in the phenomenon of slip-flow for momentum transport and requires more complex model for mass transport. Whereas these effects may be neglected in highly permeable media, many tight formations are well within this transition region under typical atmospheric temperature and pressure.

2.1. Momentum Transport

2.1.1. Viscosity

The viscosity of a fluid is a measure of the rate at which momentum is transferred to adjacent particles. For a Newtonian fluid, the viscosity, η, is the linear relationship between the shear stress and the shear velocity gradient, $\nabla\bar{u}$. Combining this shear stress with pressure and gravitational forces – that is mass density, ρ, times the gravitational field strength, $\bar{g}$ – yields the Navier-Stokes equation:

$$\rho\left(\frac{\partial\bar{u}}{\partial t} + \bar{u}\cdot\nabla\bar{u}\right) = \eta\nabla^2\bar{u} - \nabla P + \rho\bar{g}$$

The diffusive effect of viscosity is evident. Exact solutions are rare for this equation as it is nonlinear with velocity, however one such solution is the Hagen-Poiseuille equation which relates the pressure drop for steady-state flow through a cylindrical tube:

$$Q = \frac{\pi d^4}{128\eta}\frac{dP}{dz}$$

The primary takeaway is that the volumetric flow rate, Q, is dependent on pore radius to the fourth power. A rudimentary model of the porous media is a series of tubes, interconnected in three dimensions. Dividing the Hagen-Poiseuille equation by the

cross-sectional area of a cylinder and combining with the ideal gas equation of state allows the molar flux in a pore, $\bar{N}$, to be expressed:

$$\bar{N} = \frac{d^2}{32\eta} n \nabla P$$

2.1.2. Permeability

For porous media, it is not clear what the diameter of the pores would be. Clearly, the number and size of pores has a direct bearing on the molar flux. In addition, the flow must circumnavigate the solid phase, thus distributing the pressure drop over a larger distance and reducing the steady state flux. Despite these complications, it has been experimentally demonstrated, for modest flowrates, that the volumetric flow rate follows Darcy's Law (Bear 1972). Combined with the ideal gas law, Darcy's Law predicts the following molar flux:

$$\bar{N} = -n \frac{\bar{\bar{\kappa}}}{\eta} \cdot \nabla P$$

The quantity $\bar{\bar{\kappa}}$ is the permeability of the porous media. When compared with the Hagen-Poiseuille equation, it is evident that the permeability accounts for the number, size, and tortuosity of the pores normal to the pressure gradient. Strictly speaking, the permeability is a tensor quantity, as anisotropic media may have bedding planes with very different permeability in different directions.

An additional difficulty arises for gases as the mean free path approaches that of pore diameter. Whereas gas particles in the center of the pore collide with only other gas particles, gas particles near the edges collide much more frequently with solid surfaces. As the mass of the solid particles is far greater than any gas particle, the kinetic energy and hence speed of the gas particle is largely unaffected by the collision. Klinkenberg described this phenomenon as slip flow and demonstrated that by applying a species-specific correction factor, b_i, to the permeability, Darcy's Law can be applied at modest Knudsen numbers (Klinkenberg 1941).

$$\kappa_i = \kappa_\infty \left(1 + \frac{b_i}{P}\right)$$

As evident by the above equation, in the limit of high pressure, the gas permeability, κ_i, of species i approaches that of the intrinsic liquid permeability, κ_∞.

As the Klinkenberg correction demonstrates, there is a chemical specificity to the permeability. Also, while not explicitly stated earlier, the viscosity is also dependent upon the composition. Given the complexity of the gas-gas and gas-solid interactions, the gases utilized in this work will consist of a nearly pure carrier, here nitrogen, with only minor – approximately 1% or less – tracer gas components.

In doing so, the momentum balance will be satisfied in using the properties of the carrier only. That is, applying the Klinkenberg correction for the carrier, c, the momentum driven flux is as follows:

$$\bar{N}_C = -n\frac{\kappa_\infty}{\eta_c}\left(1+\frac{b_c}{P}\right)\nabla P$$

2.2. Mass Transport

2.2.1. Chemical Potential

While the most widely known driving force is the concentration gradient, chemical diffusion more precisely is driven by chemical potential. Chemical potential is a measure of the change in free energy of a system with a change in the quantity of material. Clearly, any addition or removal of material will carry the internal and potential energy of the material with it, but it will also alter the entropy of the system.

For an ideal gas, the internal energy of each particle is a function of temperature only. However, the entropy depends upon the number and type of particles confined to the system. It can be shown that entropy decreases with increasing pressure and mole fraction. Here the chemical potential is expressed accounting for the ideal gas internal energy, μ_i^0, total pressure, mole fraction, y_i, and gravitational potential.:

$$\mu_i(P,T,y_i,z) = \mu_i^0(T) + RT\ln y_i P + m_i\bar{g}z$$

Here, the gravitational potential is expresses as a function of the molar weight, m_i, the gravitational field strength, $\bar{g}$, and the elevation, z.

2.2.2. Dusty Gas Model

Provided with the chemical potential, diffusion in a pore can be described using the Dusty-Gas Model, an extension of Maxwell-Stefan diffusion for porous media. The Maxwell-Stefan model equates the chemical potential of each gas species to the frequency and magnitude of collisions with other gas species via the diffusion coefficient. Consequently, there is a linear system of equations, one for each gas species:

$$-y_i\frac{\nabla\mu_i}{RT} = \sum_{j=1,j\neq i}^{N}\frac{y_j\bar{N}_i - y_i\bar{N}_j}{nD_{ij}}$$

While useful for gaseous systems, the situation is more complex as collisions with solid surfaces become significant. The Dusty-Gas Model extends the Maxwell-Stefan model by assuming the solid phase can be represented as an additional gas component. However, being a solid, this dusty gas has unique properties.

First, the mass of the solid dust particles is immense compared with all gas species. This ensures that the molar flux of the dust is unaffected by gas collisions. Consequently, it is convenient to designate the dust particles as the inertial frame of reference. That is, all gases in motion experience additional drag when passing through the porous medium.

Second, it is unclear how the concept of mole fraction applies to dust particles. At the same time, it is unclear what the molecular diffusivity would be given the macroscopic cross-section of dust particles. This problem is circumvented by introducing the Knudsen diffusivity, which is the effusion coefficient of the media at high vacuum. This results in the following expression (Mason and Malinauskas 1983):

$$-y_{\mathrm{i}}\frac{\nabla\mu_i}{RT}=\frac{\overline{N}_i}{nD_{iK}}+\sum_{j=1,j\neq i}^{N}\frac{y_j\overline{N}_i-y_i\overline{N}_j}{nD_{ij}}$$

While comprehensive, the dusty-gas model is often excessively detailed. With a few simplifications, an explicit expression for the chemical flux can be deduced.

The first simplification can be made by ensuring the tracers species are well diluted in otherwise pure carrier. Under these conditions, interactions between gas pairs other than the carrier can be neglected. This yields two equations, the first for the carrier and the second for all other species:

$$-\frac{\nabla\mu_c}{RT}=\frac{\overline{N}_c}{nD_{cK}}$$

$$-y_i\frac{\nabla\mu_i}{RT}=\frac{\overline{N}_i}{nD_{iK}}+\frac{\overline{N}_i-y_i\overline{N}_c}{nD_{ic}}$$

At low Knudsen number, the carrier gas molar flux is better described using Darcy's Law and the Klinkenberg correction. However, at high Knudsen number, the flux of the carrier can be equivalently described by either method.

The second simplification is to assume isothermal, and nearly isobaric conditions for the tracer species. In addition, for the length scales considered here, the gravitational potential is negligible. This enables the chemical potential gradient to be express in terms of mole fraction alone.

$$\nabla_{PT}\mu_i=\frac{RT}{y_i}\nabla y_i$$

This, combined with the dilute dusty-gas model equation allows for an explicit expression of the molar flux as a function of mole fraction:

$$\overline{N}_i=\frac{1}{1+\frac{D_{ic}}{D_{iK}}}(y_i\overline{N}_c-nD_{ic}\nabla y_i)$$

Where the Knudsen diffusivity is small, the advective flux is altered by collisions with the solid surfaces. In contrast, for large Knudsen diffusivities, this formulation reverts to the Advective-Diffusive Model:

$$\overline{N}_i=y_i\overline{N}_c-nD_{ic}\nabla y_i$$

For convenience, the Advective-Diffusive Model will be used for the analytical model and deviations from idealized behavior will be compared against the Dusty-Gas Model corrections.

2.2.3. *Effective Diffusivity*

Whereas the previous section details mass flux within a pore, additional complexities arise when scaling to porous media. First, only a fraction of the surface normal to the concentration gradient is left unoccupied by the solid. The fraction of the area normal to the concentration gradient is the areal porosity that, for isotropic media, is equal to the bulk porosity. For media with bedding planes, the areal porosity may vary dramatically depending on the incident angle to the sample surface. Here, the, ε, volumetric porosity is assumed to be equal to the areal porosity:

$$\varepsilon = \frac{V_{pore}}{V_{total}}$$

Additionally, the distance the tracer must transit is highly dependent upon the connectivity of the pores. Some pathways may be more direct while others follow circuitous loops. The tortuosity, τ, is the empirical factor that compensates for the indirect pathways the particle travels and the dampening of the gradient over those pathways. It is proportional to the distance travelled in the pore versus the displacement in the absence of the porous media. However, as the actual path travelled is not known, and varies under different conditions, the parameter has only a tenuous definition (Clennell 1997).

Thus, the mean flux across a porous media sample is necessarily less than the area times the pore diffusivity. Expressing the mean flux as the integral of the pore flux incident on a surface area, $\bar{A}$:

$$\frac{\bar{N}_i}{\bar{A}} = \oint \frac{y_i \bar{N}_j - nD_{ij}\nabla y_i}{1 + \frac{D_{ij}}{D_{iK}}} \cdot d\bar{A}$$

Clearly, the net rate of transport is equal to this integral, and while the average flux can be easily observed experimentally, evaluating the integral is not readily achievable. For one, the advective component is not constant across the surface of the media, e.g., the flow at the center of the pore is faster than flow near the walls. This results in mechanical dispersion (Taylor 1953). Additionally, pores with similar velocities may have different tortuosity, leading to additional dispersion. Due to the very low advective flow rates in this work, dispersion effects are assumed to be negligible here.

Even neglecting the advective flow, the surface integral is still complex due to the obstruction posed by the solid media. Rather than attempting to evaluate the diffusivity at all positions, it is assumed there is an effective diffusivity, $\mathfrak{D}_i$, that, if employed in place of the pore diffusivity, account for these obstructions:

$$n\mathfrak{D}_i \nabla \mathrm{y_i} \cdot \bar{A} = \oint nD_{ij}\nabla y_i \cdot d\bar{A}$$

Conventionally, the ratio of the effective diffusivity to the unobstructed diffusivity is known as the porosity-tortuosity factor, or more rarely, the obstruction factor Q (Abu-El-Sha'r and Abriola 1997).

$$\frac{\mathfrak{D}_i}{D_{ij}} = \frac{\varepsilon}{\tau^2} = Q$$

Many attempts have been made at relating the obstruction factor or porosity-tortuosity factors to more readily available measurements. For example, the work of (Troeh, Jabro and Kirkham 1982) compiles at least 20 proposed models, as well as proposing a new formulation.

However, caution must be exercised with any of these models, as they are each developed for a singular class of materials, and where the pore dimensions or distributions vary considerable from material to material, the model may not be well suited. Given the scarcity of literature data on volcanic tuffs, which are in abundance in proximity to the UNESE test bed, the experimental work here attempts to measure the effective diffusivity of these samples, as well as the obstruction factor.

This page is intentionally left blank.

3. EXPERIMENTAL METHOD

To estimate the self-diffusivity of uranium hexafluoride, Ney and Armistead developed a method by which the concentration in two relatively large volumes changes when connected by a capillary tube (Ney and Armistead 1947). Because of the limited cross-sectional area of the capillary, the rate at which material is transported is limited despite large concentrations differences. By sizing the chambers and capillary appropriately, it can be ensured that a linear concentration gradient sets in the capillary far faster than concentration changes in the end bulbs – the quasi-steady-state approximation. Additionally, because of the adjustable relaxation time, the experiment can be designed to accommodate lengthy batch analytical techniques.

Using a variation of this method, Paul et al. demonstrated that this quasi-steady-state approximation could also be applied to porous geological media (Paul, Biegalski, et al. 2018). In this case, the material under test replaces the capillary restriction. Whereas the analysis is complicated as the material under test may not have a negligible volume, by withdrawing aliquots from both ends of the apparatus, the equilibrium concentration can be determined where the volume of the system is unknown.

Both previous references rely on discrete sampling, which is both labor intensive and prone to operator errors. In this work, a quadrupole mass spectrometer (Pfeiffer HiQuad QMA 410) was employed for continuous monitoring. A schematic is shown in Figure 3-1. Continuously Monitored Quasi-Steady-State Apparatus. Whereas this provides an essentially limitless number of samples, reducing numerical uncertainty, this comes as the cost of more significantly perturbing the system. That is, when combined with the quadrupole mass spectrometer, the system is no longer truly a closed system. Therefore, a correction for the advective component must be made to extract the diffusivity.

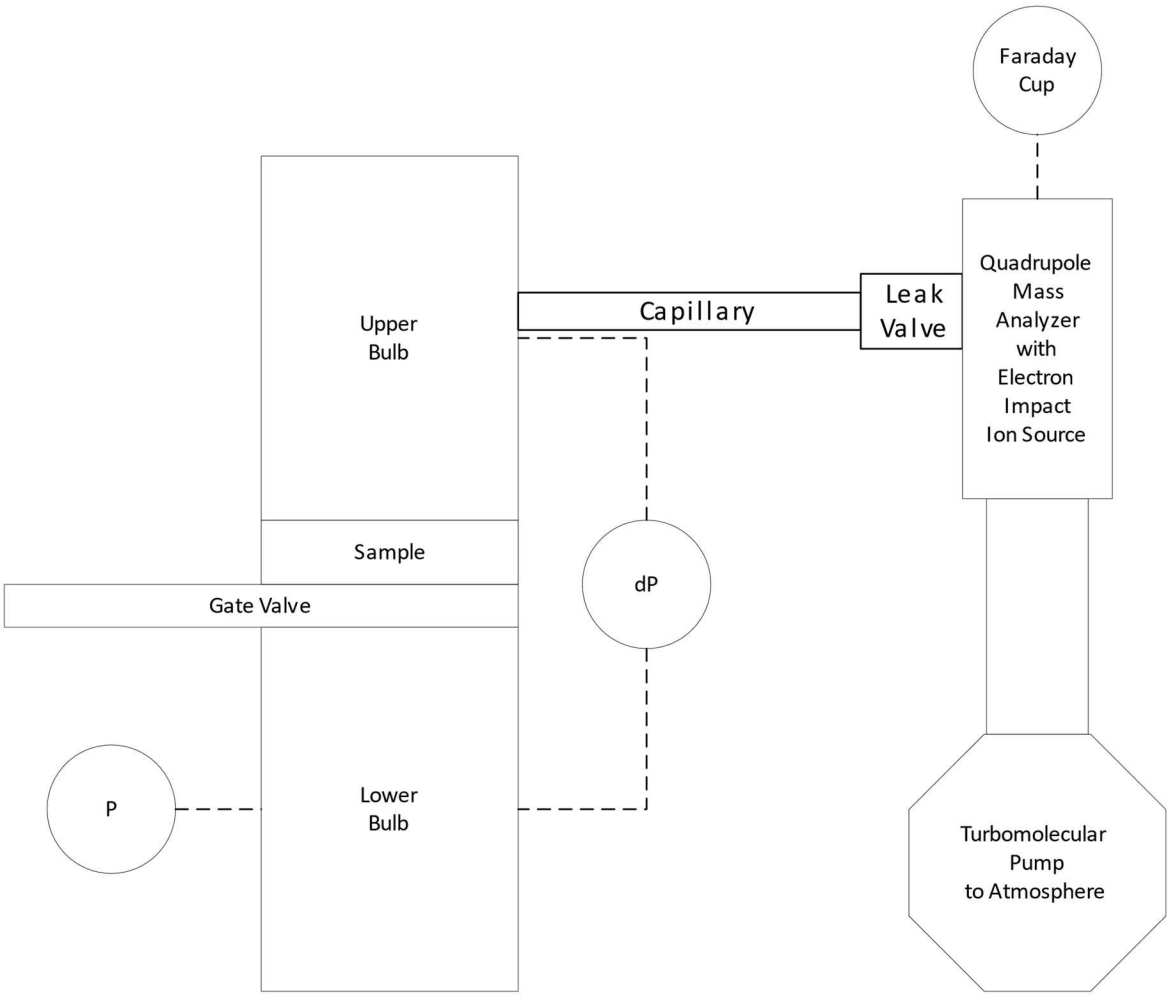

Figure 3-1. Continuously Monitored Quasi-Steady-State Apparatus

3.1. Total Species Balance

As the apparatus is constructed of rigid stainless steel, each region of the system effectively has a constant volume. In addition, temperature in the system, while not strictly isothermal, is maintained within a narrow range of ambient conditions. Using the ideal gas law, the quantity of gas in each chamber can be represented as the product of concentration and constant chamber volume.

Given that the quadrupole mass spectrometer operates at approximately 10^{-5} mbar, despite its sizeable volume, it does not appreciably contribute to the total mass balance. However, over time, the quantity of material that is evacuated by the turbomolecular pump is non-negligible.

Therefore, only two material balances are necessary, one for the lower and upper chamber. Flow through the porous media is expressed as $\dot{N}_p$ while flow to the quadrupole is expressed as $\dot{N}_q$.

$$\begin{aligned} V_\ell \frac{dn_\ell}{dt} &= -\dot{N}_p \quad +0 \\ V_u \frac{dn_u}{dt} &= +\dot{N}_p \quad -\dot{N}_q \end{aligned}$$

Flow through the porous media can be calculated via Darcy's Law. Given the small pressure gradient across the media, compressibility effects across the porous media will be neglected. In addition, it is presumed that the contribution from the Klinkenberg effect is approximately constant over the narrow range of pressures considered. Letting the conductivity, K_P represent the combination of intrinsic permeability, κ_∞, the Klinkenberg correction factor, $1 + b_c/P$, viscosity, μ, cross-sectional area, A, and length, L:

$$\dot{N}_p = -n\frac{\kappa_\infty}{\eta_c}\left(1 + \frac{b_c}{P}\right)\frac{A}{L}\Delta P = nK_p\Delta P$$

In contrast to the Darcy flow across the porous media, massive decompression occurs across the variable leak valve. As the quadrupole is constantly operated at high vacuum – 10^{-5} mbar or less - flow on the downstream side will always be limited by Knudsen flow. While the size of the aperture is variable and unknown, it is nevertheless constant during the experiment. Letting C_q represent the vacuum conductivity, the molar flow rate to the quadrupole is as follows:

$$\dot{N}_q = nC_q$$

As the conductivity of the porous media is far greater than the conductivity of the leak valve to the quadrupole chamber, the differential pressure negligibly alters the total pressure. Summing these two material balances together yields a single differential equation that is a function of the quadrupole flow rate:

$$\frac{V_\ell + V_u}{RT}\frac{dP}{dt} - \frac{V_u}{RT}\frac{d\Delta P}{dt} = -\dot{N}_q$$

At quasi-steady state, the time derivative of differential pressure is considerably smaller than the time derivative of total pressure. Nullifying the differential pressure yields a linear, first-order differential equation for total pressure:

$$\frac{1}{P}\frac{dP}{dt} = -\frac{C_q}{V_\ell + V_u} = -k_q$$

For brevity, k_q will be used to represent the leak valve conductivity over total system volume. Given this notation, the pressure of the system will follow the trivial solution:

$$P(t) = P(0)e^{-k_q t}$$

With this solution and transient pressure data, the flow coefficient to the quadrupole can be estimated by fitting a simple exponential curve.

If, instead of taking the summation of the two molar balances, the difference is taken, an expression for the change in differential pressure can be found:

$$\frac{d\Delta P}{dt} = -K_p P \Delta P \left(\frac{1}{V_\ell} + \frac{1}{V_u}\right) + C_q \frac{P}{V_u}$$

At quasi-steady state, the time derivative of differential pressure is negligible. With this approximation, the Darcy flow across the sample can be solved in terms of Knudsen flow to the quadrupole chamber:

$$\dot{N}_p = \frac{V_\ell}{V_\ell + V_u}\dot{N}_q = nk_q V_\ell$$

That is, under quasi-steady-state conditions, each chamber is depleted of material at a rate proportional to its share of the total volume. This in turn is a function of the molar concentration, the rate of pressure decay, and the lower chamber volume.

3.2. Tracer Species Balance

In addition to the total species balance, which is dominated by the carrier gas, each tracer species must independently be conserved. At quasi-steady state, accumulation in the porous media is negligible and the concentration gradient can be approximated by the differential across the two chambers. The molar flux of a tracer species across the porous media is, using the advective-diffusive model:

$$\dot{N}_{i,p} = y_i \dot{N}_p + n\mathcal{D}_i \frac{A}{L}\Delta y_i$$

Whereas diffusion can occur in the line to the quadrupole, a stainless-steel capillary was chosen to ensure the mean cross-sectional area versus length is very small. By maintaining a sufficient mean velocity in the capillary, the diffusive component can be neglected. Therefore, flow to the quadrupole is represented as:

$$\dot{N}_{i,q} = y_i \dot{N}_q$$

Since the advective flow in this arrangement is unidirectional, this enables the molar balance of each species to be written as follows:

$$\begin{aligned} V_\ell \frac{dy_{i,\ell} n_\ell}{dt} &= 0 - y_{i,\ell}\dot{N}_P - n\mathfrak{D}_i \frac{A}{L}\left(y_{i,\ell} - y_{i,u}\right) \\ V_u \frac{dy_{i,u} n_u}{dt} &= -y_{i,u}\dot{N}_Q + y_{i,\ell}\dot{N}_P + n\mathfrak{D}_i \frac{A}{L}\left(y_{i,\ell} - y_{i,u}\right) \end{aligned}$$

Provided with direct measurements of concentration, these equations would be solved directly. However, the ion current in a mass spectrometer is linearly proportional to concentration in the quadrupole chamber, albeit also on electron impact cross section, transmission efficiency, filament current, vacuum pressure and so on. For example, as the flow rate of the leak valve decreases with diminishing system pressure, it is expected that the vacuum pressure will change with time, altering the ion currents.

Rather than repeatedly calibrating the instrument as flow rates and sensitivities shift, a more practical solution is to take the ratio of the tracer species ion current, I_i, to a reference species ion current, I_c. Provided that the instrument response is linear for each species, this ratio is proportional to the mole ratio. In addition, where the reference species is representative of the carrier, and the tracer species is dilute, the mole ratio is proportional to the mole fraction.

$$y_i \propto \frac{I_i}{I_c}$$

Provided only a single instrument is used per trial, it is not necessary to quantity the instrument response function. As the tracer species balances are homogeneous with mole fraction, the gain of the response function factors out exactly. For brevity, the remaining derivations will retain the mole fraction notation with the understanding that the ion current ratio can be used as a proxy for these quantities.

At this point, it is necessary to express the advective flows using the relationships derived for the total species balance.

$$\begin{aligned} V_\ell \frac{dy_{i,\ell} n_\ell}{dt} &= 0 - y_{i,\ell} n k_q V_\ell - n\mathfrak{D}_i \frac{A}{L}\left(y_{i,\ell} - y_{i,u}\right) \\ V_u \frac{dy_{i,u} n_u}{dt} &= -y_{i,u} n k_q (V_\ell + V_u) + y_{i,\ell} n k_q V_\ell + n\mathfrak{D}_i \frac{A}{L}\left(y_{i,\ell} - y_{i,u}\right) \end{aligned}$$

To determine solve this equation, the time derivative of the molar fraction must be isolated from the molar concentration. Dividing both equations by the ideal gas equation of state and, assuming isothermal conditions, the following separated equations result:

$$\begin{aligned} V_\ell \left(y_{i,\ell} \frac{1}{P}\frac{dP}{dt} + \frac{dy_{i,\ell}}{dt}\right) &= 0 - y_{i,\ell} k_q V_\ell - \mathfrak{D}_i \frac{A}{L}\left(y_{i,\ell} - y_{i,u}\right) \\ V_u \left(y_{i,u} \frac{1}{P}\frac{dP}{dt} + \frac{dy_{i,u}}{dt}\right) &= -y_{i,u} k_q (V_\ell + V_u) + y_{i,\ell} k_q V_\ell + \mathfrak{D}_i \frac{A}{L}\left(y_{i,\ell} - y_{i,u}\right) \end{aligned}$$

The eigenvalue from the total species balance can be used to eliminate the remaining pressure dependency. This greatly simplifies the system into a system of two linear differential equations:

$$V_\ell \frac{dy_{i,\ell}}{dt} = -\mathfrak{D}_i \frac{A}{L} \left(y_{i,\ell} - y_{i,u}\right)$$
$$V_u \frac{dy_{i,u}}{dt} = \left(k_q V_\ell + \mathfrak{D}_i \frac{A}{L}\right) \left(y_{i,\ell} - y_{i,u}\right)$$

A system such as this can be expressed concisely in matrix-vector form. Dividing through by the corresponding chamber volume:

$$\frac{d}{dt}\begin{bmatrix} y_{i,\ell} \\ y_{i,u} \end{bmatrix} = \begin{bmatrix} -\frac{1}{V_\ell}\mathfrak{D}_i \frac{A}{L} & +\frac{1}{V_\ell}\mathfrak{D}_i \frac{A}{L} \\ \frac{1}{V_u}\left(k_q V_\ell + \mathfrak{D}_i \frac{A}{L}\right) & -\frac{1}{V_u}\left(k_q V_\ell - \mathfrak{D}_i \frac{A}{L}\right) \end{bmatrix} \cdot \begin{bmatrix} y_{i,\ell} \\ y_{i,u} \end{bmatrix}$$

The eigenvalues, k, for this matrix system are:

$$k = 0 \; or \; -\left(k_q \frac{V_\ell}{V_u} + \mathfrak{D}_i \frac{A}{L} \frac{V_\ell + V_u}{V_\ell V_u}\right)$$

It is evident here that the first eigenvalue represents the equilibrium condition and will be consistently null for all tracers. Consequently, the unknown coefficient for this eigenvector will be annotated as $y_{i,\infty}$. The second eigenvector, henceforth denoted as $-k_{\mathrm{i},\Delta}$, is a summation of the advective and diffusive contributions. As the diffusive component varies by species, there is an eigenvalue for each tracer. Together, with the corresponding eigenvectors, and the unknown coefficients – $y_{i,\infty}$ and $y_{i,\Delta}$ – the general solution is:

$$\begin{bmatrix} y_{i,\ell} \\ y_{i,u} \end{bmatrix} = y_{i,\infty} \begin{bmatrix} 1 \\ 1 \end{bmatrix} + y_{i,\Delta} \begin{bmatrix} -\mathfrak{D}_i \frac{A}{L}\frac{1}{V_\ell} \\ k_q \frac{V_\ell}{V_u} + \mathfrak{D}_i \frac{A}{L}\frac{1}{V_u} \end{bmatrix} e^{-k_{\mathrm{i},\Delta} t}$$

Although the continuous removal of material does perturb the system, deviating from the methodology of Ney-Armistead, the analytical solution for mole fraction is only slightly more complex. Provided with independent pressure and volume measurements to calculate the advective contribution, the relaxation time analogous to the closed system method can be readily determined:

$$k_{i,\Delta} - k_q \frac{V_\ell}{V_u} = \mathfrak{D}_i \frac{A}{L} \frac{V_\ell + V_u}{V_\ell V_u}$$

Perhaps the greatest complexity introduced is that the equilibrium mole fraction cannot be calculated without prior knowledge of the advective and diffusive contributions. Thus, the above solution must be solved without knowledge of $y_{i,\infty}$. Note that, for sorbent porous media, this was already problematic as the quantity of material in the media is non-negligible (Paul, Biegalski, et al. 2018). Therefore, while this method

requires more complex curve fitting than the method of Ney and Armistead, the uncertainty introduced can be overcome by the far greater number of samples possible versus batch sampling.

3.3. Procedures

To achieve a pure carrier gas phase, the upper and lower chambers are ensured to be pneumatically connected by opening an equalization bypass valve in parallel to the differential pressure transducer. The system is then pumped to vacuum using a Pfeiffer MVP 040 diaphragm pump. The chambers are then backfilled to approximately 900 mbar using ultra-high purity nitrogen (> 99.999% Matheson). This process is repeated three times to remove residual tracer gases from prior tests.

For partially saturated porous media samples, the pressure diminishes to near the vapor pressure of water – approximately 30 mbar. To ensure the partially saturated samples are not dried by this procedure, a wetted paper towel is added to both chambers. The water on the paper acts as a kinetically favorable source of water vapor at vacuum. In this way, when the vacuum pressure approaches the vapor pressure of water, the water is primarily evaporating from the paper rather than the porous media. The effectiveness of this method can be confirmed by weighing the porous media samples before and after the test procedure.

The gate valve and equalization valve are then shut. Using a Hamilton 1010SL gas-tight syringe, 10.0 mL of each tracer at approximately 3000 mbar is injected into a septum connected to the lower chamber. To prevent losses due to permeation or septum failure, an isolation valve is located between the septum and the lower chamber. The lower chamber is then allowed to internally diffuse for a minimum of 16 hours.

Pressure and temperature are measured at one second intervals throughout the experiment using an inhouse LabVIEW program. The absolute pressure is measured using a Pfeiffer CMR361 capacitive manometer with a range of 0-1100 mbar. The total pressure signal is then digitized using a Pfeiffer Maxigauge controller. Similarly, the differential pressure is measured using an MKS 226 differential pressure capacitance manometer with a range of 0-20 torr differential. The MKS gauge is powered and the signal processed by the MKS PDR2000. Both the Pfeiffer Maxigauge and MKS PRD2000 are interfaced to a Windows PC using RS-232 serial bus interfaces. Additionally, temperature is also recorded using an Omega PR-25AP 100Ω Platinum resistance temperature detector. Current to this sensor was supplied and voltage measured using a National Instruments 9217 C module installed in a National Instruments cDAQ-9188. This in turn was linked to the LabVIEW program via ethernet bus. Given the timing is at one-second intervals, the internal clock on the computer is sufficient.

At the same time, the mass spectrometer ion current is monitored for the tracer and carrier species. A one second dwell time is allotted for each channel. The reference ion current channel chosen corresponds to a mass-to-charge ratio of 14, which corresponds to a dissociated nitrogen molecule. Channels 40 and 132 are used for argon and xenon respectively, as these correspond to the single ionization peak of the most abundant isotope. Sulfur hexafluoride dissociates upon ionization. Consequently, channel 127 is

utilized, which corresponds to the most abundant isotopologue after the removal of a single fluorine atom. Additionally, channel 32, corresponding to oxygen, is also recorded to diagnose air infiltration. In all cases, the Faraday Cup collector is utilized as it permits a higher operating pressure of up to 10^{-4} mbar.

For the wet tests, the leak valve aperture is adjusted so that the pressure in the vacuum chamber was approximately 10^{-5} mbar. For dry tests, which have far faster transients, the leak valve is adjusted closer to 10^{-4} mbar. This increase in flow rate reduces the transit time in the capillary, ensuring the ion current measured is representative of the molar fraction in the upper chamber. In both cases, the leak valve flow rate is calculated by the rate of pressure decay in the chamber.

The test duration varied upon the ion current response. It is numerically desirable for the ion current ratios to approach equilibrium to provide the greatest confidence in diffusivity. However, the very low diffusivity in some materials prevented the gases from approaching equilibrium even after several weeks. Given time constraints on the equipment, it was necessary to terminate some trials prior to reaching equilibrium to allow testing of additional samples.

4. RESULTS

Thirteen trials were carried on eight different core samples. Five of these samples were repeated with as-delivered and oven-dried water content. Given the fragility of some samples, it was not possible to repeat the trial after oven drying. Additionally, air was observed to have leaked into sample 'UE-12p#4 626.3-627.1 (wet, thick) ZN'. Hence, the total pressure did not decrease as anticipated by the above model.

The figures on the following pages depict the observed pressure in the system and ion current ratios, referenced to the nitrogen carrier, with time.

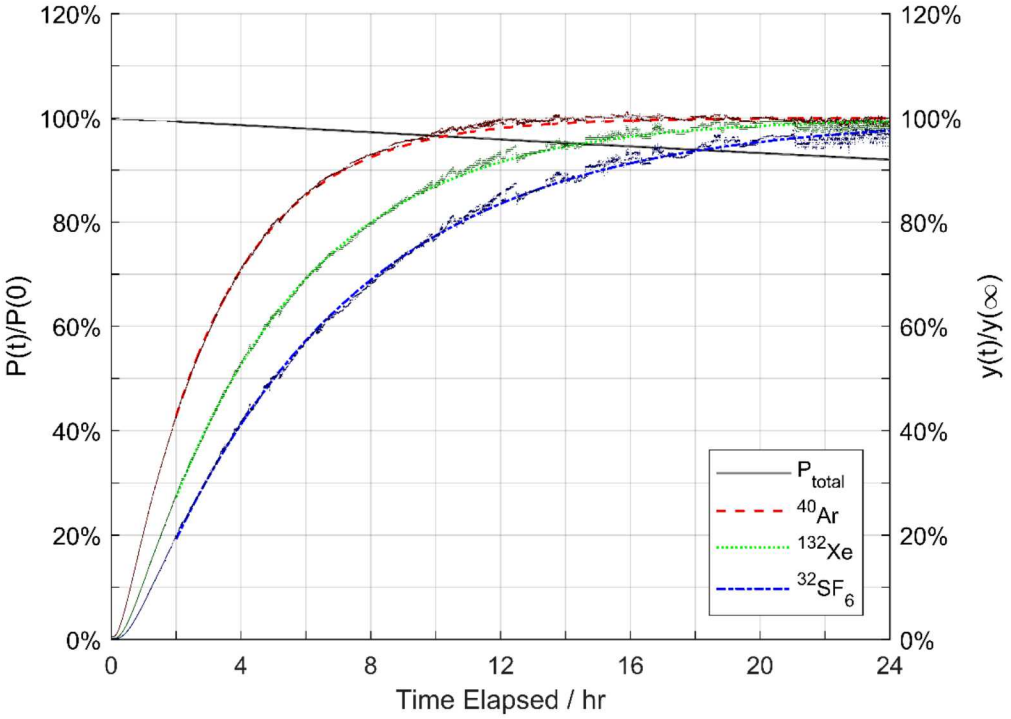

Figure 4-1. U12p.03 RE-7 10.4-10.7 (dry, thin) ZN

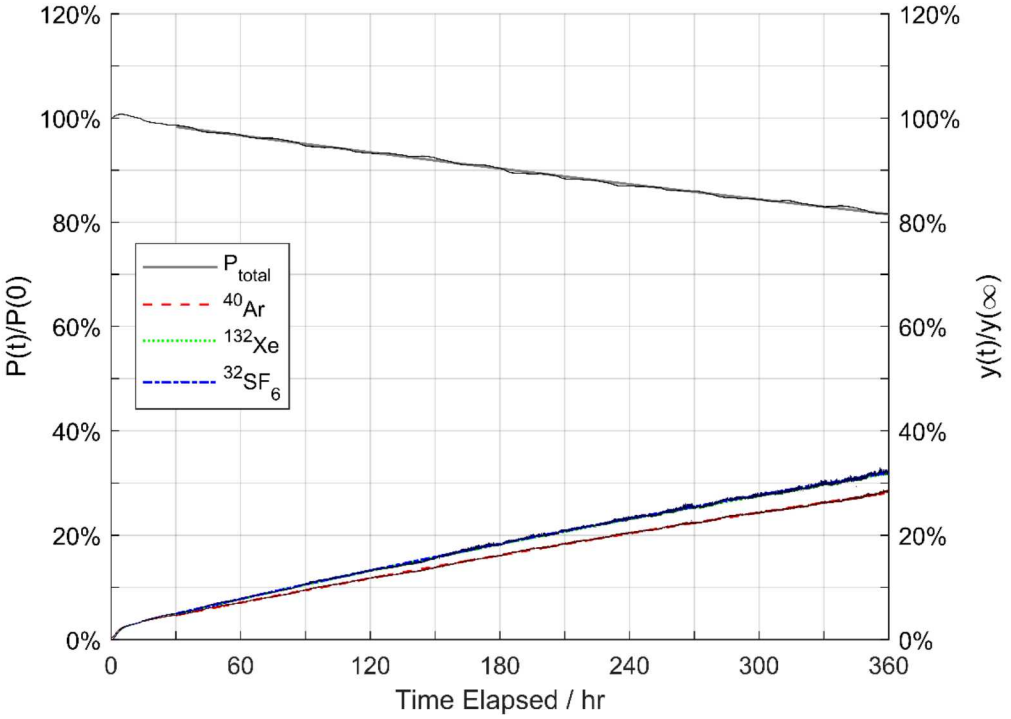

Figure 4-2. U12p.03 RE-7 10.4-10.7 (wet, thin) ZN

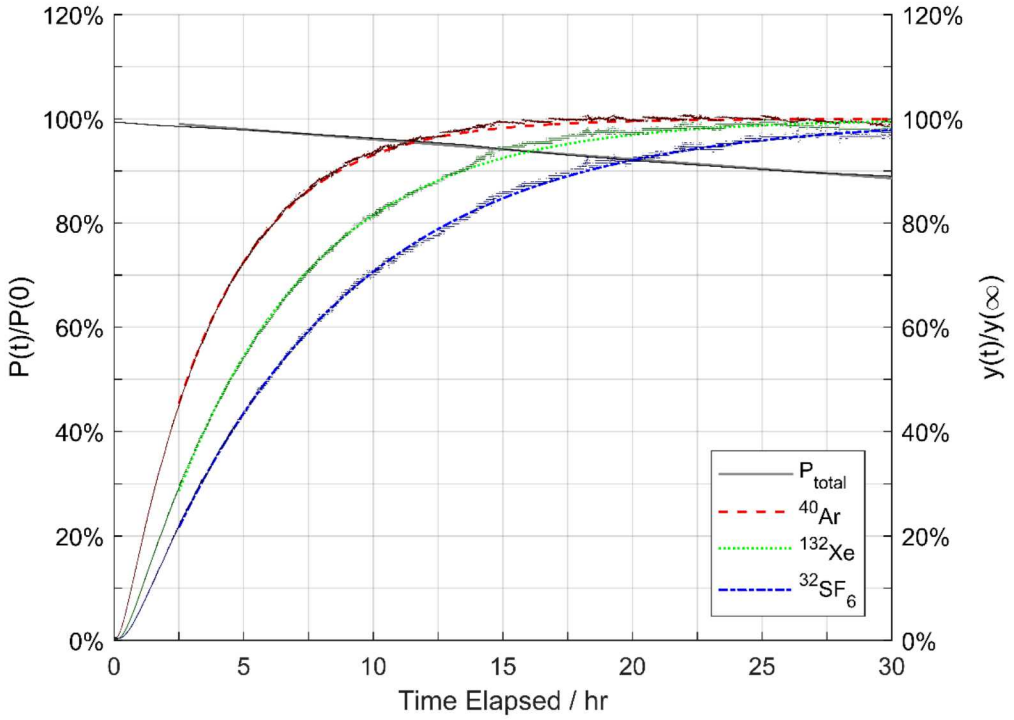

Figure 4-3. U12p.03 RE-7 14.9-15.5 (dry, thin) ZN

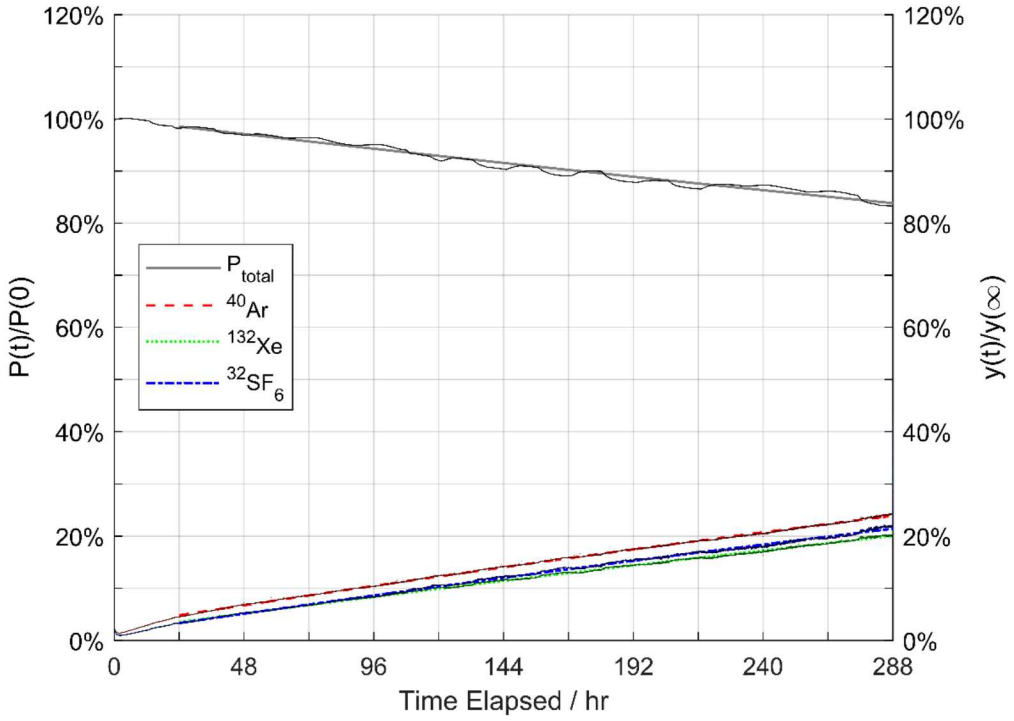

Figure 4-4. U12p.03 RE-7 14.9-15.5 (wet, thin) ZN

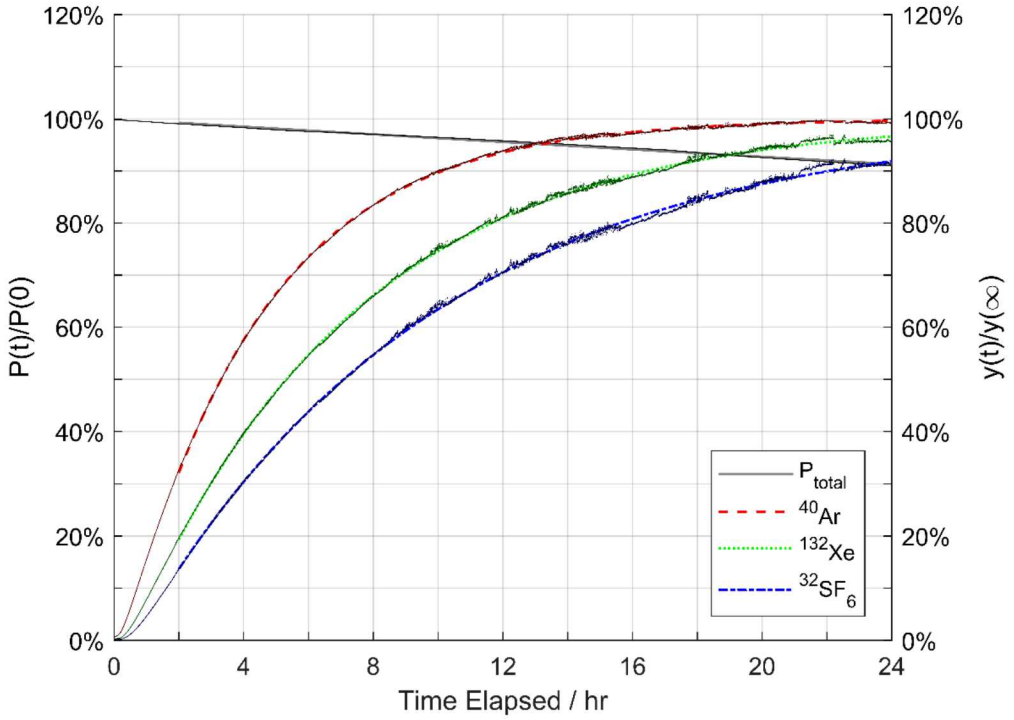

Figure 4-5. U12p.03 RE-7 38.6-39.6 (dry, thin) ZN

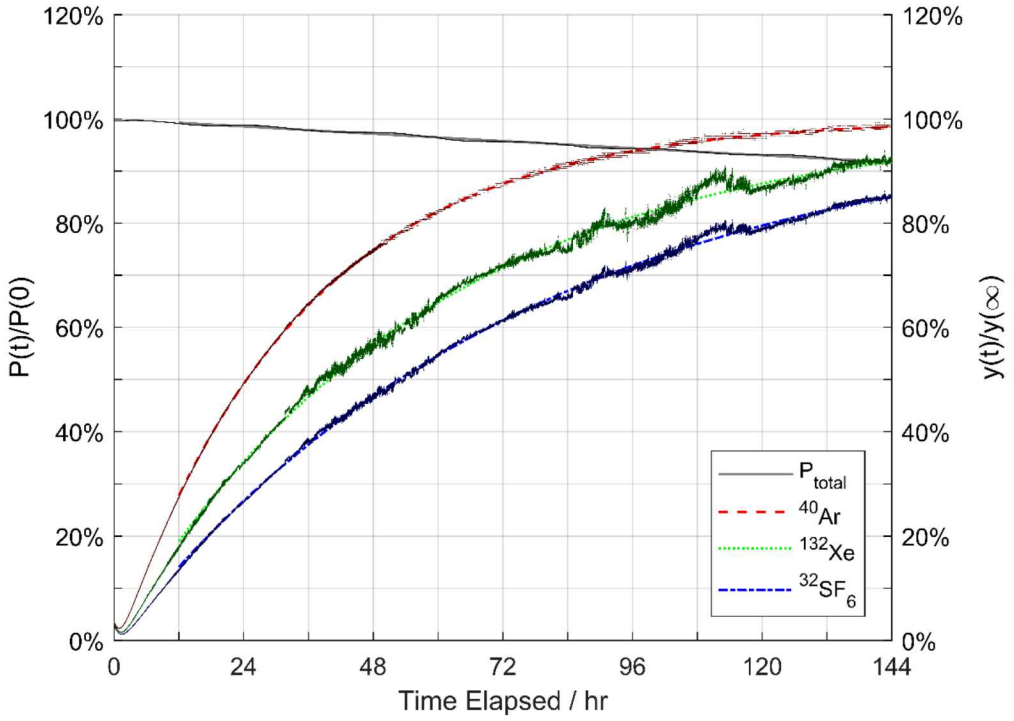

Figure 4-6. U12p.03 RE-7 38.6-39.6 (wet, thin) ZN

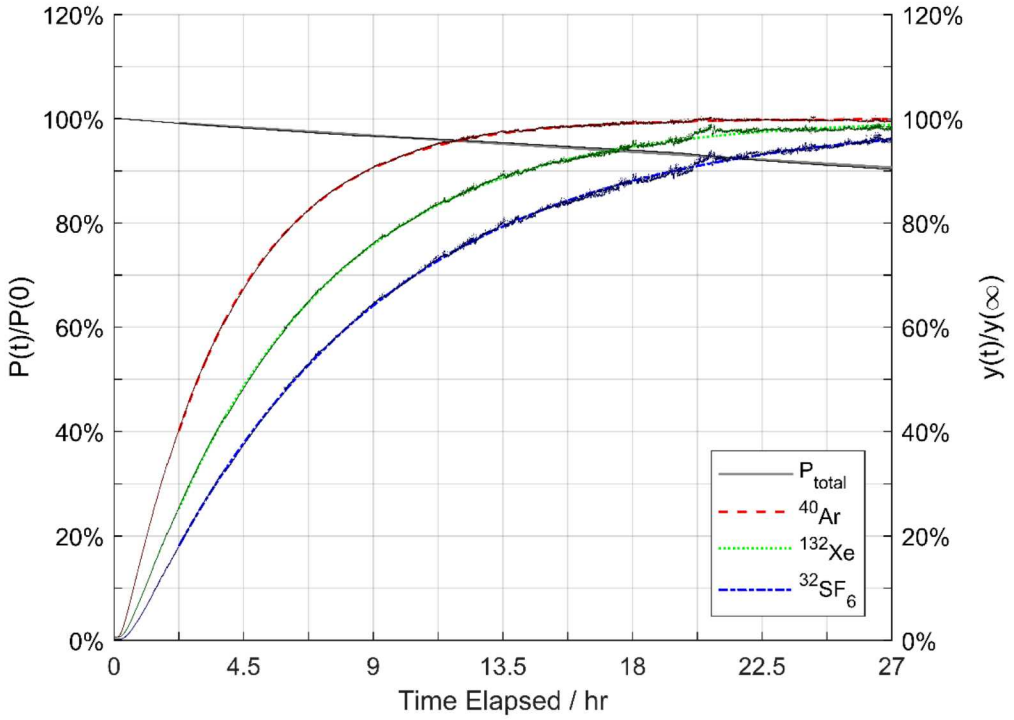

Figure 4-7. U12p.03 RE-7 82.4-82.9 (dry, thin) ZN

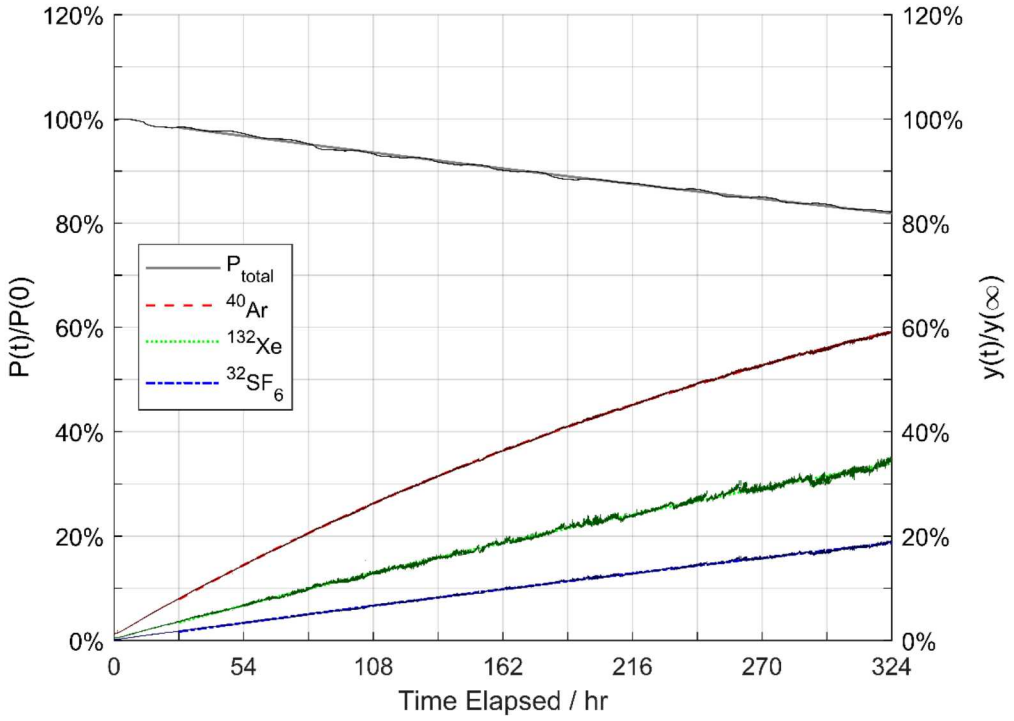

Figure 4-8. U12p.03 RE-7 82.4-82.9 (wet, thin) ZN

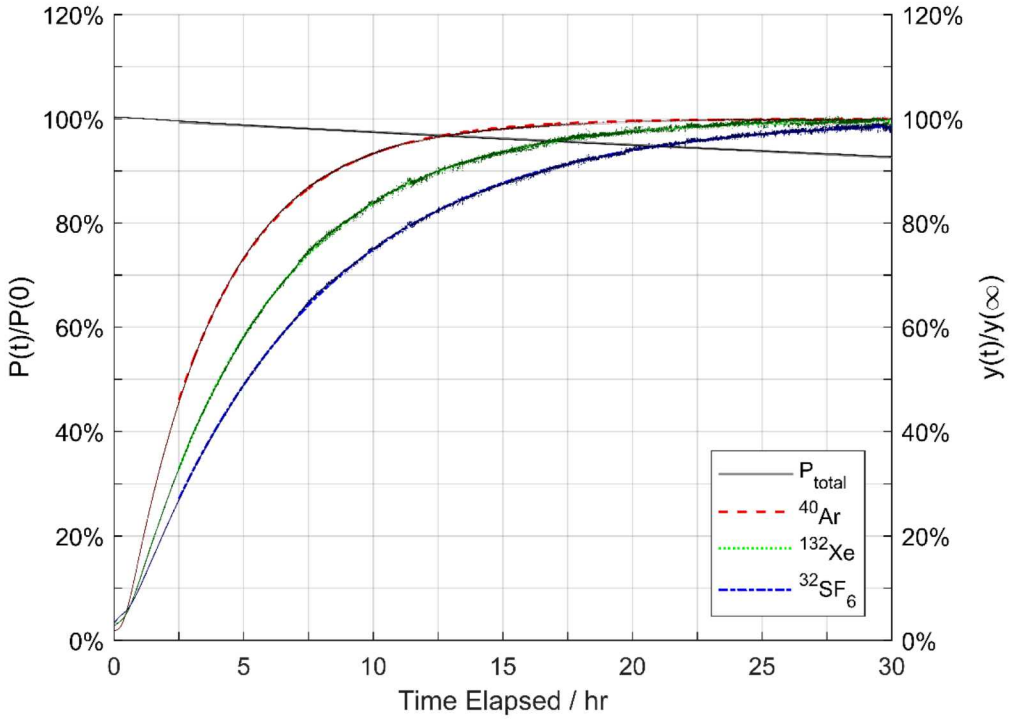

Figure 4-9. UE-12p#4 140.8-141.7 (dry, thin) PW

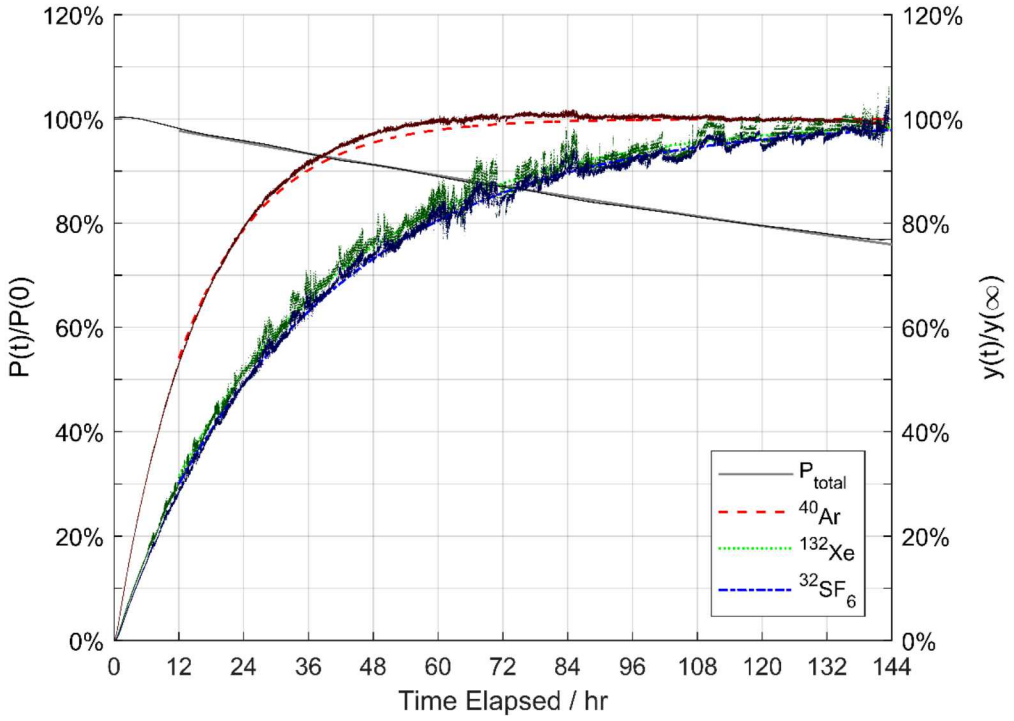

Figure 4-10. UE-12p#4 367.2-368.2 (dry, thin) SW

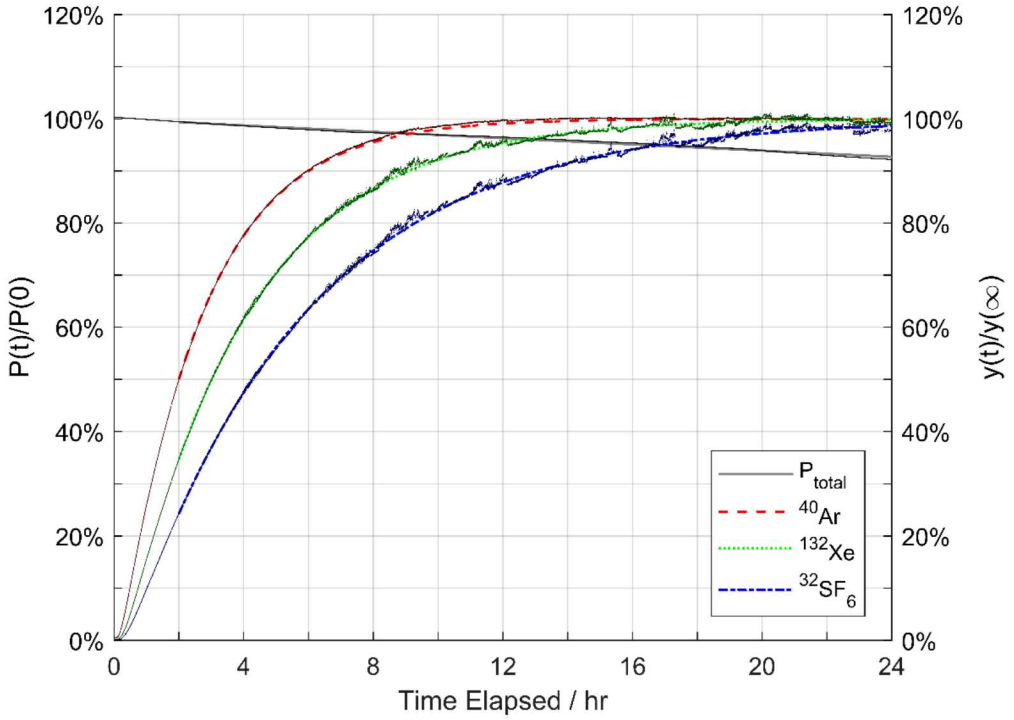

Figure 4-11. UE-12p#4 780.1-780.6 (dry, thin) ZN

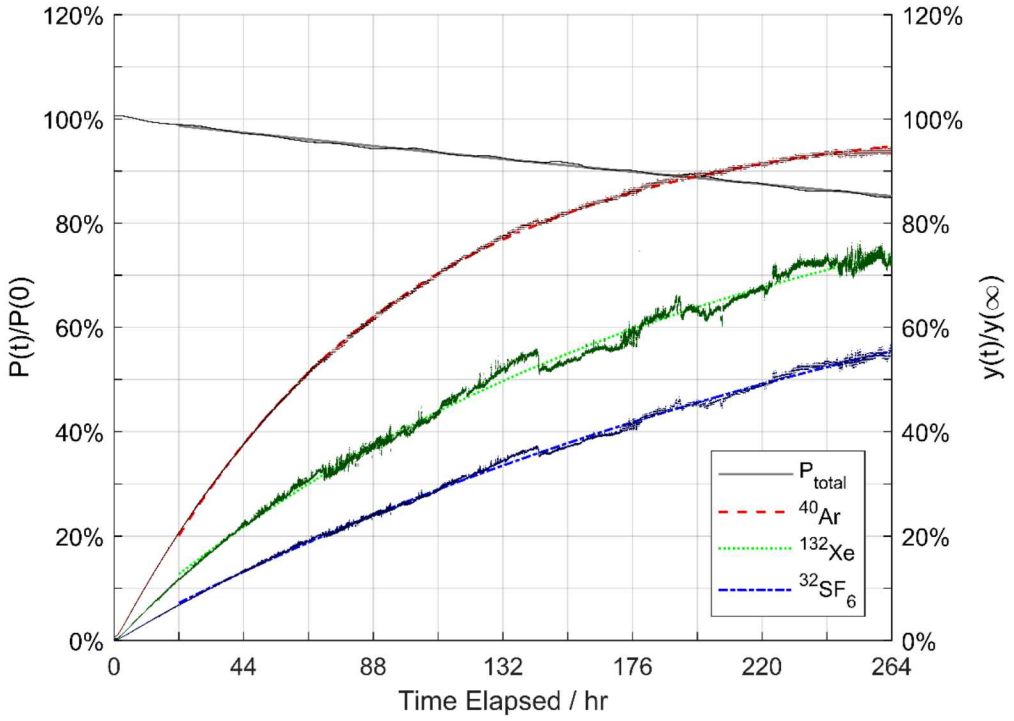

Figure 4-12. UE-12p#4 780.1-780.6 (wet, thin) ZN

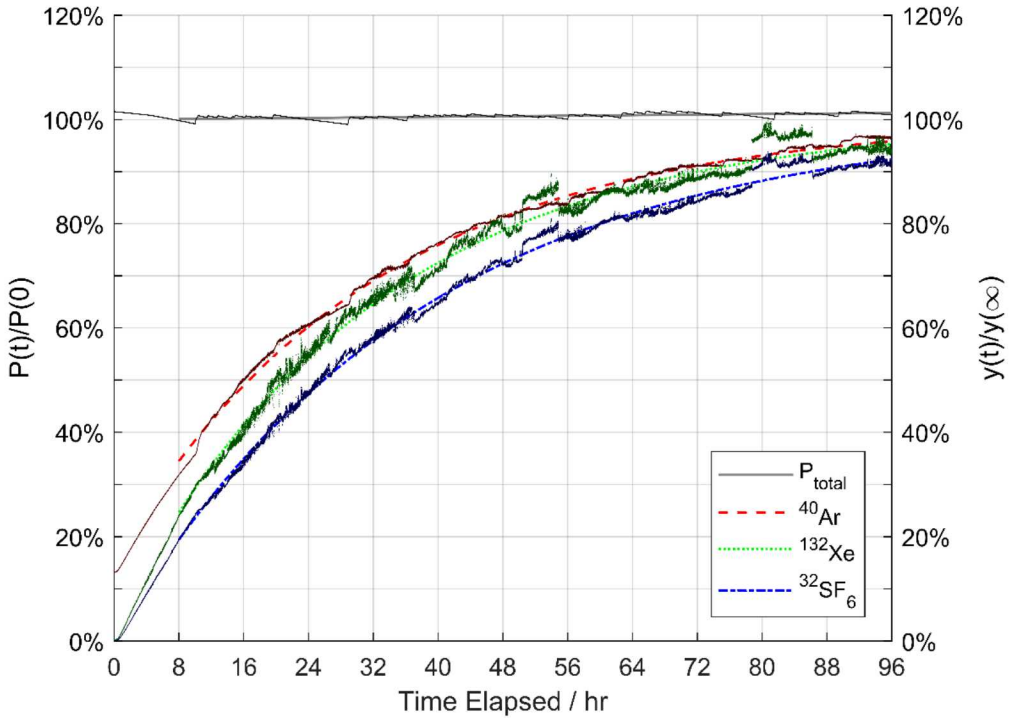

Figure 4-13. UE-12p#4 626.627.1 (wet, thick) VN

As observed in Figure 4-13, the pressure did not decay as anticipated. Additionally, the argon results show an unexpectedly high initial mole fraction, further suggesting that air has infiltrated the system. Whereas these results show qualitatively that the transport rates are as expected, because it is not possible to quantity the rate of air infiltration, the numerical results will be excluded from discussion.

4.1. Fitted Parameters

As discussed in section 3, the quasi-steady-state model predicts exponential time responses for both total pressure and ion current ratios. As early in the experimental time, the quasi-steady-state conditions have not set in, the first $1/12^{th}$ of each data set is omitted from curve fitting. The fitted curves have been shown on figures in the preceding section represented by dashed lines of the same color as the data.

The maximum likelihood estimate was used assuming normally distributed error for both pressure and ion current ratios (Paul 2017). Additionally, the unknown equilibrium ion current ratio was estimated using a golden search algorithm (Kiefer 1953) to minimize the squared residuals. The MATLAB functions are provided in Appendix A. The resulting characteristic time constants are reported in Table 4-1. Characteristic Times.

Sample	$1/k_q$ (hr)	$1/k_{i,\Delta}$ (hr)		
		^{40}Ar	^{132}Xe	$^{32}SF_6$
U12p.03 RE-7 10.4-10.7 (dry, thin) ZN	286	2.96	4.65	6.29
U12p.03 RE-7 10.4-10.7 (wet, thin) ZN	1767	1168.59	993.93	986.16
U12p.03 RE-7 14.9-15.5 (dry, thin) ZN	248	3.64	5.56	7.64
U12p.03 RE-7 14.9-15.5 (wet, thin) ZN	1633	1181.67	1407.89	1275.25
U12p.03 RE-7 38.6-39.6 (dry, thin) ZN	264	4.25	6.92	9.31
U12p.03 RE-7 38.6-39.6 (wet, thin) ZN	1663	34.17	57.56	75.27
U12p.03 RE-7 82.1-82.9 (dry, thin) ZN	275	3.66	5.96	8.17
U12p.03 RE-7 82.1-82.9 (wet, thin) ZN	1621	364.60	783.83	1568.59
UE-12p#4 140.8-141.7 (dry, thin) PW	390	3.59	5.27	7.02
UE-12p#4 367.2-368.2 (dry, thin) SW	522	15.55	35.06	37.56
UE-12p#4 780.1-780.6 (dry, thin) ZN	317	2.49	3.78	5.48
UE-12p#4 780.1-780.6 (wet, thin) ZN	1648	88.85	199.54	329.71

Table 4-1. Characteristic Times

These characteristic times can be combined with measured bulb and sample dimensions to calculate the effective diffusivity. Table 4-2. Sample Dimensions below lists the macroscopic dimensions of the core samples under test.

Sample	Length (cm)	Diameter (cm)
U12p.03 RE-7 10.4-10.7 ZN	0.724	6.256
U12p.03 RE-7 14.9-15.5 ZN	0.480	6.330
U12p.03 RE-7 38.6-39.6 ZN	0.480	6.330
U12p.03 RE-7 82.1-82.9 ZN	1.537	6.299
UE-12p#4 140.8-141.7 PW	0.602	6.040
UE-12p#4 367.2-368.2 SW	0.345	6.083
UE-12p#4 780.1-780.6 ZN	1.052	5.977

Table 4-2. Sample Dimensions

Table 4-3. Chamber Volumes lists the chamber volumes measured using pressure response to measured syringe additions.

Chamber	Volume (cm^3)
Lower	2635
Upper	5443

Table 4-3. Chamber Volumes

With these parameters, it is possible to calculate the effective diffusivity from the characteristic times. Table 4-4 lists the estimates for each of the twelve successful trials.

Sample	Effective Diffusivity (cm^2/hr) ^{40}Ar	^{132}Xe	$^{32}SF_6$
Nitrogen at 25 C (Marrero and Mason 1972)	704.18	452.03	344.22
U12p.03 RE-7 10.4-10.7 (dry, thin) ZN	14.04	8.91	6.58
U12p.03 RE-7 10.4-10.7 (wet, thin) ZN	0.02	0.03	0.03
U12p.03 RE-7 14.9-15.5 (dry, thin) ZN	7.39	4.82	3.49
U12p.03 RE-7 14.9-15.5 (wet, thin) ZN	0.01	0.01	0.01
U12p.03 RE-7 38.6-39.6 (dry, thin) ZN	6.32	3.86	2.86
U12p.03 RE-7 38.6-39.6 (wet, thin) ZN	2.54	1.50	1.14
U12p.03 RE-7 82.1-82.9 (dry, thin) ZN	23.79	14.53	10.56
U12p.03 RE-7 82.1-82.9 (wet, thin) ZN	0.16	0.07	0.02
UE-12p#4 140.8-141.7 (dry, thin) PW	10.35	7.03	5.26
UE-12p#4 367.2-368.2 (dry, thin) SW	1.34	0.58	0.54
UE-12p#4 780.1-780.6 (dry, thin) ZN	26.61	17.49	12.05
UE-12p#4 780.1-780.6 (wet, thin) ZN	0.73	0.31	0.18

Table 4-4. Effective Diffusivity

First, in all cases, the effective diffusivity is more than an order of magnitude less than the free nitrogen diffusivity. Consequently, while the chambers were not mechanically agitated, because the diffusivity in the samples was so obstructed, it is confirmed that the end chambers were nevertheless well mixed by passive diffusion.

Second, diffusivity in the oven-dried samples is considerably larger than in the as-delivered wet samples. Roughly speaking, the effective diffusivity dropped by two orders of magnitude for all tracer species. Water content thereby has a significant impact on effective diffusivity.

To evaluate if the impact is chemically selective or is purely a physical effect, the ratio of the effective diffusivity to the free nitrogen diffusivity is taken to determine the porosity-tortuosity factor. A tight alignment indicates the porosity-tortuosity factor is sufficient to account for the porous media whereas a spread of data points indicates the internal pore diffusivity may have been altered.

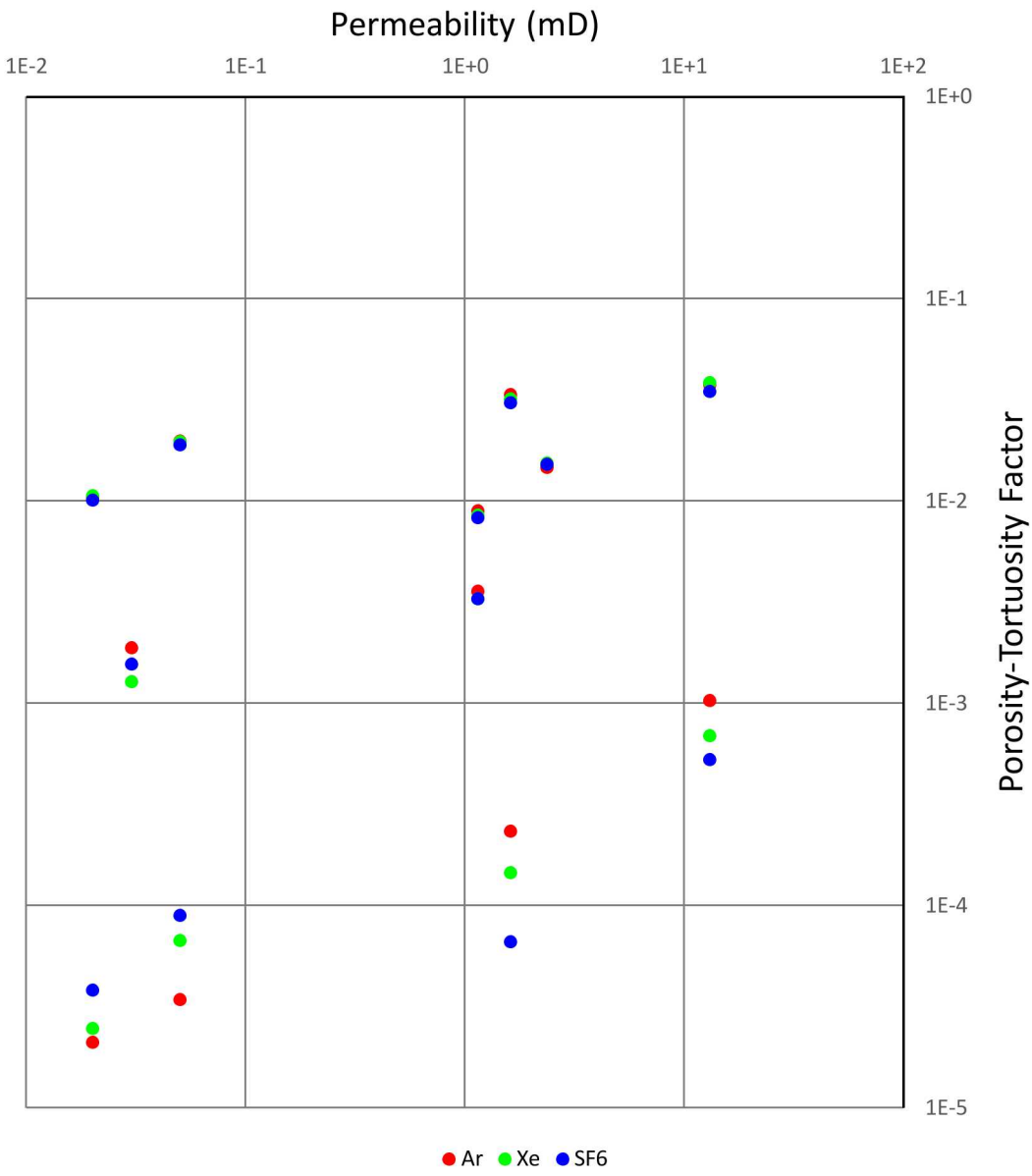

Figure 4-14. Porosity-Tortuosity Factor versus Permeability

Where the porosity-tortuosity factor is above 0.001, there is a strong grouping between the tracer species and their nitrogen diffusivities. Interestingly, there is no clear correlation between the porosity-tortuosity factor and reported permeabilities. While diffusivity is largely proportional to areal porosity, permeability is, in contrast, proportional to areal porosity weighted by pore radius squared. Consequently, it appears that a few fractures or macropores account for the majority of the advective flow while the diffusive flow occurs over the broader base of micropores. This result is, however, limited to the volcanic tuff considered in this study.

At lower porosity-tortuosity factors, larger deviations are observed between the tracer species. While it is abundantly clear that the diffusivity was lowered substantially, it must also be cautioned that these tests were terminated far before reaching equilibrium. Consequently, it is not possible at this time to conclude if these differences represent chemically selective transport due to the presence of water or fall within experimental uncertainties or if they are within the uncertainty of the experiment.

5. CONCLUSION

This work encompasses both an advancement in the techniques to characterize diffusivity in porous media samples as well as utilizable measurements on the geologic materials in the proximity of the UNESE venture.

First, this methodology has demonstrated a reliable method to measure the effective diffusivity of virtually any gas across porous media using a quadrupole mass spectrometer. Previous methods relied on molecular spectroscopy – which is unsuitable for noble gases – or limited batch samples to minimize material losses. With few assumptions, this method permits estimation of effective diffusivity while compensating for the advection induced by the sample withdrawn. In addition, provided the rate of evaporation is slower than the diffusion time, this methodology permits estimation of the effective diffusivity of partially saturated media. With refined estimates for the diffusivity of wetted samples, the apparatus can be resized to reduce execution time and provide more precise parameter estimates.

Second, the samples under test have demonstrated that diffusivity has only a weak relationship with permeability. Whereas this conclusion is limited to tuff, the ramification is that matrix elements that make a negligible contribution to advective flows may nevertheless contribute substantially to diffusive flows. Therefore, caution must be made when scaling models from highly advective flows to stagnant or oscillatory flows.

Additionally, these results show a dramatic shift in the effective diffusivity under wetted and dried conditions. The primary function of the retained water appears to be physically blocking diffusion pathways. Whereas some difference in nitrogen diffusivity ratios was observed, leaving open the possibility for some chemical selectivity, this difference was near the precision of the method.

Future work will focus on improving precision, evaluating the uncertainty, and reducing the execution time of the experiment. These changes will enable testing of a broader range of samples and increased fidelity in the parameters needed for accurately modeling subterranean gas migration.

This page is intentionally left blank.

REFERENCES

Abu-El-Sha'r, Wa'il, and Linda M. Abriola. 1997. "Experimental assessment of gas transport mechanisms in natural porous media: Parameter evaluation." *Water Resources Research* 33 (4): 505-516. doi:10.1029/96WR03536.

Bear, Jacob. 1972. *Dynamics of Fluids in Porous Media.* New York: American Elsevier.

Carrigan, C. R., R. A. Heinle, G. B. Hudson, J. J. Nitao, and J. J. Zucca. 1996. "Trace gas emissions on geological faults as indicators of underground nuclear testing." *Nature* 382 (6591): 528-531. doi:10.1038/382528a0.

Chapman, Sydney, and T. G. Cowling. 1970. *The mathematical theory of non-uniform gases: An account of the kinetic theory of viscosity, thermal conduction and diffusion in gases.* 3rd ed. Cambridge, Eng.: Cambridge University Press.

Clennell, M. Ben. 1997. "Tortuosity: a guide through the maze." *Geological Society, London, Special Publications* 122 (1): 299-344. doi:10.1144/GSL.SP.1997.122.01.18.

Kiefer, J. 1953. "Sequential minimax search for a maximum." *Proceedings of the American Mathematical Society* 4 (3): 502-506. doi:10.2307/2032161.

Klinkenberg, L. J. 1941. "The permeability of porous media to liquids and gases." *Drilling and Production Practice.* New York: American Petroleum Institute. 200-213.

Marrero, T. R., and E. A. Mason. 1972. "Gaseous diffusion coefficients." *Journal of Physical and Chemical Reference Data* 3-118. doi:10.1063/1.3253094.

Mason, E. A., and A. P. Malinauskas. 1983. *Gas transport in porous media: The dusty-gas model.* New York: Elsevier.

Ney, Edward P., and Fontaine C. Armistead. 1947. "The self-diffusion coefficient of uranium hexafluoride." *Physical Review* 71 (1): 14-19. doi:10.1103/PhysRev.71.14.

O'Hanlon, John F. 2003. *A user's guide to vacuum technology.* 3rd ed. Hoboken, NJ: Wiley-Interscience.

Olsen, K. B., R. R. Kirkham, V. T. Woods, D. A. Haas, J. C. Hayes, T. W. Bowyer, D. P. Mendoza, and et al. 2016. "Noble gas migration experiment to support the detection of underground nuclear explosions." *Journal of Radioanalytical and Nuclear Chemistry* 307 (3): 2603-2610. doi:10.1007/s10967-015-4639-7.

Paul, Matthew J. 2017. *Transport and sorption of noble gases in porous geological media.* PhD dissertation, Austin: University of Texas.

Paul, Matthew J., Steven R. Biegalski, Derek A. Haas, and Justin D. Lowrey. 2018. "Adsorptive transport of noble gas tracers in porous media." *International Journal of Modern Physics: Conference Series* 48: 1860124. doi:10.1142/S2010194518601242.

Taylor, Geoffrey I. 1953. "Dispersion of soluble matter in solvent flowing slowly through a tube." *Proceedings of the Royal Society of London, Series A, Mathematical and Physical Sciences* 219 (1137): 186-203. doi:10.1098/rspa.1953.0139.

Troeh, Frederick R., Jalal D. Jabro, and Don Kirkham. 1982. "Gaseous diffusion equations for porous materials." *Geoderma* 27 (3): 239-253. doi:10.1016/0016-7061(82)90033-7.

United Nations. 1996. "Comprehensive Nuclear Test-Ban Treaty." New York. https://www.ctbto.org/fileadmin/content/treaty/treaty_text.pdf.

This page is intentionally left blank.

APPENDIX A: MAXIMUM LIKELIHOOD ESTIMATE SEARCH ALGORITHM

```
function [A,B,C,err] = fit_exp_c(x,y)
%% MLE for an exponential curve fit with constant offset.
%% Error weighted normally in linear space.
%% Iterate via golden search to find the minimum.

%% Fibonacci number
phi = (1+sqrt(5))/2;
%% Tolerance on C
tol = 0.0000001;

%% Calculate initial guess using last 1% of values
C = sum(y(floor(.99*length(y)):end))/(length(y)-floor(.99*length(y))+1);

%% Setup four point probe, using 1 decade range.
a = 1.0*C;
b = 10.0*C;
c = b - (b-a)/phi;
d = a + (b-a)/phi;

while abs(c-d) > tol
    [A_c,B_c,err_c] = fit_exp(x,c-y);
    [A_d,B_d,err_d] = fit_exp(x,d-y);

    if (err_c < err_d)
        b = d;
    else
        a = c;
    end

    c = b - (b-a)/phi;
    d = a + (b-a)/phi;
end

C = (a + b) / 2;
[A,B,err] = fit_exp(x,C-y);

End
```

```
function [A,B,err] = fit_exp(x,y)
%% MLE for an exponential curve fit. Error weighted normally in linear space.
%%
xyy   = sum(x.*y.^2,'omitnan');
xxyy  = sum(x.^2.*y.^2,'omitnan');
xyyly = sum(x.*y.^2.*log(y),'omitnan');
yyly  = sum(y.^2.*log(y),'omitnan');
yy    = sum(y.^2,'omitnan');

A = real((xxyy*yyly-xyy*xyyly)/(yy*xxyy-xyy^2));
A = exp(A);
B = real((yy*xyyly-xyy*yyly)/(yy*xxyy-xyy^2));

err = abs(y - A*exp(B*x));
err = sum(err.^2);

end
```

DISTRIBUTION

1	MS0404	Neill Symons	06752
1	MS0735	Joshua Feldman	08864
1	MS0735	Moo Lee	08864
1	MS0747	Kristopher Kuhlman	08844
1	MS0750	Nancy Brodsky	08865
1	MS0750	Jason Heath	08864
1	MS0751	Richard Jensen	08864
1	MS1033	Scott Broome	08864
1	MS1033	Matthew Paul	08865
1	MS0899	Technical Library	9536 (electronic copy)


Sandia National Laboratories